Applied Catalysis B: Environmental 150–151 (2014) 107–115

Contents lists available at ScienceDirect

Applied Catalysis B: Environmental

journal homepage: www.elsevier.com/locate/apcatb

# Correlation study between photo-degradation and surface adsorption properties of phenol and methyl orange on $TiO_2$ Vs platinum-supported $TiO_2$

J.J. Murcia[a,*], M.C. Hidalgo[a], J.A. Navío[a], J. Araña[b], J.M. Doña-Rodríguez[b]

[a] Instituto de Ciencia de Materiales de Sevilla (ICMS), Consejo Superior de Investigaciones Científicas CSIC—Universidad de Sevilla, Américo Vespucio 49, 41092 Sevilla, Spain
[b] CIDIA (Departamento de Química), Universidad de las Palmas de Gran Canaria, Edificio del Parque Científico Tecnológico, Campus Universitario de Tafira, 35017 Las Palmas de Gran Canaria, Spain

ARTICLE INFO

*Article history:*
Received 13 September 2013
Received in revised form 4 December 2013
Accepted 6 December 2013
Available online 14 December 2013

*Keywords:*
$Pt–TiO_2$
FT-IR
Phenol
Methyl orange
Substrate adsorption

ABSTRACT

Adsorption of phenol and methyl orange on the surface of $TiO_2$ and $Pt–TiO_2$ photocatalysts was investigated by FT-IR spectroscopy. It was found that platinum plays an important role in the adsorption properties of the studied substrates on $TiO_2$. Platinum deposits modified the phenol-photocatalyst interaction providing new adsorption sites on $TiO_2$ surface. On $Pt–TiO_2$ photocatalysts, phenol mainly interacts via formation of adsorbed phenolates species. It was also found that the adsorption of methyl orange on titania and $Pt–TiO_2$ photocatalysts occurs via interaction of the azo group with surface $Ti^{4+}$. Pt photodeposition significantly increases the $TiO_2$ photoreactivity in phenol and methyl orange photo-degradation; however, this increase depends on the properties of the Pt deposits. Moreover, it was observed that platinum content is the main factor determining the substrate-photocatalyst interaction and therefore the $Pt–TiO_2$ photocatalytic performance.



## 1. Introduction

The search for improving the $TiO_2$ efficiency as photocatalyst has revealed that titania modified by deposition of platinum and other noble metals is an interesting method for the enhancement of $TiO_2$ activity in the photo-oxidation of a wide variety of organic and inorganic substrates [1–9]. The photocatalytic efficiency of titania is determined, in part, by the electron–hole pairs lifetime; that should be long enough to allow interfacial charge-transfer reactions. Platinum acts as a trap for electrons, forming a charge transfer complex between Pt and $TiO_2$. However, when the amount of Pt is high, $TiO_2$ activity may also decrease. It is well accepted that Pt clusters in a low number act as separation centers; as photogenerated electrons are transferred from $TiO_2$ conduction band to the Pt deposits and holes are accumulated in the $TiO_2$ valence band, being efficiently separated. However, a large number of Pt deposits may act as recombination centers. The recombination rate between electrons and holes increases with the increase of Pt content, as the average distance between trap sites decreases by increasing the number of Pt clusters confined within a particle [1,10,11].

It has also been reported that the improvement of $TiO_2$ photoactivity by Pt addition depends not only on Pt content but also on $TiO_2$ properties, metal particle size and Pt oxidation state [1,12–15]. Moreover, adsorption properties of a specific substrate may be different on bare $TiO_2$ than on Pt loaded $TiO_2$ and this also has a direct influence on photoactivity; and this issue has been less studied.

In a recent paper some of us have described an approach for controlling the features of platinum deposits on $TiO_2$ prepared by photodeposition [4]. Platinum particle size and valence state seemed to be the main factors influencing the improvement of the $TiO_2$ photo-activity in the phenol and methyl orange (MO) degradation reactions. These factors were controlled by changing the photodeposition time during the preparation method.

The goal of the present study is to gain fundamental knowledge about the interaction substrate-photocatalyst when $TiO_2$ is metalized, correlating the adsorption results with the behavior observed during the photocatalytic degradation of phenol and methyl orange. A qualitative FT-IR study about the adsorption of these molecules on $TiO_2$ and platinized $TiO_2$ was attempted.

## 2. Experimental

### 2.1. Preparation of photocatalysts

#### 2.1.1. Sol–gel synthesis of $TiO_2$

Titanium tetraisopropoxide (Aldrich, 97%) (TTIP) was used as precursor for the sol–gel synthesis. This process was carried out

* Corresponding author. Tel.: +34 954489550; fax: +34 954460665.
*E-mail addresses:* jjuliejoseane@hotmail.com, juliejmm@cartuja.csic.es (J.J. Murcia).

0926-3373/$ – see front matter © 2013 Elsevier B.V. All rights reserved.
http://dx.doi.org/10.1016/j.apcatb.2013.12.010

by controlled addition of distilled water into a well-mixed TTIP-isopropanol solution (1.6 M), with volume ratio isopropanol/water 1:1. The $TiO_2$ powder was recovered by filtration and dried at 110 °C for 24 h. Afterward, the dry powder was sulfated by immersion in a 1 M sulfuric acid solution under continuous stirring for 1 h, followed by filtration, drying and calcination at 650 °C for 2 h.

#### 2.1.2. Platinized $TiO_2$

The procedure of platinum deposition on $TiO_2$ was based on previous results [4]. Pt photodeposition was performed using an aqueous solution of hexachloroplatinic acid ($HPtCl_6$, Aldrich 99.9%) containing isopropanol, which acts as sacrificial donor where the $TiO_2$ was suspended (2 g/L). The amount of Pt precursor was selected to be 0.5% and 2% respect the $TiO_2$ total weight. This suspension was illuminated under $N_2$ atmosphere for different times (15, 120 and 240 min) using an Osram Ultra-Vitalux lamp (300 W) with sun-like radiation spectrum and a main emission line in the UVA range at 365 nm. The intensity of the lamp was 60 W/m$^2$ (determined with a PMA 2200 UVA Photometer Solar Light Co.). After photodeposition the powders were recovered by filtration and dried at 110 °C overnight.

### 2.2. Characterization of photocatalysts

Specific surface area ($S_{BET}$) of all photocatalysts was determined using low-temperature nitrogen adsorption on an ASAP 2010 instrument (Micromeritics). Absorption properties were studied by UV–vis spectroscopy using a Varian Cary 100 UV–vis spectrophotometer coupled to an integration sphere for diffuse reflectance studies. $BaSO_4$ was used as reference. Band-gaps values were calculated from the corresponding Kubelka–Munk functions ($F(R\infty)$),which are proportional to the absorption of radiation, by plotting $(F(R\infty) \times h\nu)^{1/2}$ against $h\nu$ [16].

Platinum content was ascertained by X-ray fluorescence (XRF) analysis with a Panalytical Axios sequential spectrophotometer. XRF measurements were performed onto pressed pellets (sample included in 10 wt% of wax).

X-ray diffraction (XRD) patterns were obtained on a Siemens D-501 diffractometer with Ni filter and graphite monochromator using Cu Kα radiation. Crystallite sizes were calculated from the line broadening of the main XRD peaks by using the Scherrer equation. Peaks were fitted by using a Voigt function.

X-ray photoelectron spectra were recorded using a Leybold-Heraeus LHS-10 spectrometer, working with constant pass energy of 50 eV. The spectrometer main chamber, working at a pressure $<2 \times 10^{-9}$ Torr, is equipped with an EA-200 MCD hemispherical electron analyzer with a dual X-ray source working with Al $K\alpha$ ($h\nu$ = 1486.6 eV) at 120 W and 30 mA. C 1s signal (284.6 eV) was used as internal energy reference in all the experiments. Samples were outgassed in the prechamber of the instrument at 150 °C up to a pressure $<2 \times 10^{-8}$ Torr to remove chemisorbed water. Platinum valence state was ascertained on the basis of information given in a previous publication and estimated by deconvolution of Pt $4f_{7/2}$ and Pt $4f_{5/2}$ doublets using the UNIFIT 2009 software [4,17].

Platinum particle size distribution in Pt–$TiO_2$ samples was determined by Transmission Electron Microscopy (TEM) using a Philips CM200 analytical microscope. The samples were dispersed on ethanol using an ultrasonicator and dropped on a carbon grid. Determination of the metal particle average diameter ($\bar{d}$) in the different samples was accomplished by counting particles in a high number of TEM images from different places of the samples. The following equation was used:

$$\bar{d}\,(nm) = \sum di \times fi;$$

where $di$ is the diameter of the $ni$ counted particles and $fi$ is the particle size distribution estimated by

$$fi = \frac{ni}{\sum ni}$$

where $ni$ is the number of particles of diameter $di$ [14].

Diffuse reflectance infrared Fourier transform spectroscopy (DRIFTS) spectra were recorded on a Thermo Scientific-Nicolet iS10 spectrophotometer. Intervals of 4000–1000 cm$^{-1}$, a resolution of 2 cm$^{-1}$ and a forward and reverse moving mirrors speed of 10 and 6.2 kHz, respectively, were used.

### 2.3. Dark adsorption of organics

Dark adsorption experiments of phenol and MO on $TiO_2$ and Pt–$TiO_2$ were carried out using a 2 g/L photocatalyst suspension containing the substrate, each suspension was stirred for 24 h; prior to stirring pH value was adjusted to 5.0 ± 0.05 by addition of 0.1 M NaOH or HCl solutions. After preliminary adsorption tests with different substrate concentrations, 1000 ppm of phenol and 5000 ppm of MO were chosen for this work, since these concentrations leads to IR peaks with the highest resolution for the analyzed substrates. The mixtures were filtered through a 0.5 μm pore size filter and dried at room temperature. Then, the photocatalysts were placed between two $CaF_2$ windows in a proper cell for FT-IR analysis and the spectra were recorded.

### 2.4. Evaluation of photocatalytic activity

Photocatalytic experiments were carried out using a discontinuous batch system described in detail in a previous publication [4]. This includes a 400 mL pyrex reactor enveloped by an aluminum foil, filled with an aqueous suspension (250 mL) containing 50 ppm of phenol (0.53 mM) or MO (0.15 mM) and photocatalyst (1 g/L). This system was illuminated through a UV-transparent Plexiglas® top window (threshold absorption at 250 nm) by an Osram Ultra-Vitalux lamp (300 W) with sun-like radiation spectrum and a main line in the UVA range at 365 nm. In order to favor the adsorption–desorption equilibrium, prior to irradiation the suspension was magnetically stirred for 10 min in dark. Magnetic stirring and a constant oxygen flow of 35 L/h as an oxidant were used to produce a homogeneous suspension of the photocatalyst in the solution. All photocatalytic tests started at pH ca. 6 and the total reaction time was 120 min.

During the phenol photoreaction, samples were collected at different times and measured by HPLC, using an Agilent Technologies 1200 chromatograph, which was equipped with UV–vis detector and an Elipse XDB-C18 column (5 μm, 4.6 mm × 150 mm). The HPLC analysis was carried out using water/methanol (65:35) as mobile phase, a flow rate of 0.8 mL/min and 40 °C. In order to evaluate the dye discoloration rate, the concentration of MO during the photodegradation reaction was analyzed by UV–vis spectroscopy, considering the main peak of this dye located at 460 nm [18].

Photolysis tests of phenol and MO under UV light and in absence of catalyst were carried out. Under the experimental conditions used in this work, substrate photolysis was not observed in any case. Reproducibility of the measurements was ensured by double testing of selected samples, obtaining standard error values of $4.0 \times 10^{-4}$ and $1.3 \times 10^{-4}$ in the photo-degradation of phenol and methyl orange, respectively.

## 3. Results and discussion

### 3.1. Characterization and analysis

In a previous work the control of photodeposition parameters such as deposition time and Pt content, allowed us to obtain specific

features in the Pt deposits on $TiO_2$ [4]; these features had a clear influence over the photocatalytic activity of Pt–$TiO_2$ samples tested in phenol and MO degradation. All the photocatalysts prepared were characterized extensively using different analytic techniques. In the present work we have included new characterization results and a brief summary of the more relevant already reported results for comparison purposes. In addition, a FT-IR study of the adsorption properties of all the photocatalysts for phenol and MO was performed.

The key experimental parameters used in this work and some characterization results are summarized in Table 1. As it can be observed in this table, properties of $TiO_2$ such as band gap, anatase crystallite size (see also Ref. [4]) and $S_{BET}$ were not significantly affected by Pt addition. Only a slight decrease of $S_{BET}$ with the deposition time was detected, probably due to pore blocking by metal precursor. The real platinum amount deposited on $TiO_2$ was determined by XRF and it was found that the amount of metal was lower than the nominal Pt content in all the samples; evidencing an incomplete reduction of $H_2PtCl_6$. Impurities coming from the synthesis procedure were also detected by XRF; thus, in Pt–$TiO_2$ samples a low amount of $Cl^-$ (between negligible and ca. 0.05%) and sulfur amounts (between 0.08 and 0.12%) were found.

XPS analyzes were carried out to determine the chemical and electronic structure of the samples and the valence states of Pt on the surface. Two signals located at $529.6 \pm 0.2$ eV and 530.0 eV were detected for O 1s, these signals correspond to lattice $O^{2-}$ and surface OH groups, respectively. In the Ti $2p_{3/2}$ region, peaks located at binding energies of 458.5 eV were observed and assigned to $Ti^{4+}$ in the $TiO_2$ lattice. The value of O/Ti atomic surface ratio of $TiO_2$ was 1.70, this ratio is below the stoichiometric value, suggesting the presence of a certain number of oxygen vacancies on the surface of this material. It has been reported that the sulfate pre-treatment and further calcination contributes to the formation of these vacancies [4,19]. On Pt–$TiO_2$ samples the O/Ti ratio increases, probably due to a partial annihilation of the oxygen vacancies during the platinum deposition process. XPS studies also have revealed that Pt precursor was only partially photoreduced, yielding $Pt^0$ and $Pt^{\delta+}$ species on platinized samples. It was also observed that the $Pt^0$ fraction increases as deposition time increases up to 120 min.

By XRD studies it was observed that anatase was the only crystalline phase present in all the samples; no peaks of platinum were detected, even at the highest Pt content.

Fig. 1(A) and (B) shows TEM images of Pt–$TiO_2$ samples, where black dots can be identified as platinum deposits. Inset in Fig. 1(A) is the histogram of the platinum particle size distribution in the 0.5 wt% Pt–$TiO_2$ sample prepared with 120 min of deposition time. As it can be seen, most of the particles are between 3 and 5 nm. As was reported in Table 1, for materials prepared with 0.5 wt% Pt, the average particle size ($\bar{d}$) increases with the deposition time. For samples prepared with 2 wt% of platinum loading most Pt deposits are present as large agglomerates with sizes larger than 10 nm (Fig. 1(B)). This high degree of agglomeration prevented any attempt of particle size distribution determination.

### 3.2. FT-IR measurements

A qualitative FT-IR study of all the samples was performed. Fig. 2(I) and (II) shows the spectra of $TiO_2$ and Pt–$TiO_2$ samples prepared with 0.5 and 2 wt% Pt, respectively, and deposition times between 15 and 240 min (range between 4000 and 2400 $cm^{-1}$). A band at 3698 $cm^{-1}$ corresponding to isolated hydroxyl groups (Ti–OH) was detected in all the samples [20–22,26]. In $TiO_2$ spectrum (Fig. 2 line (A)) two clear bands at 3393 and 3214 $cm^{-1}$ were identified, these bands are distinctive of the interaction of water with surface titanium atoms (Ti–$OH_2$) through hydrogen bonds. In Pt–$TiO_2$ samples, a wide band characteristic of physisorbed water can be observed, and the width of this band increases with the deposition time [22–24].

As it can be seen in Fig. 2, the relative intensity of the band assigned to isolated OH groups is slightly higher for 0.5 wt%Pt–$TiO_2$ photocatalysts (Fig. 2(I)) than for $TiO_2$ but it decreases markedly in the photocatalysts prepared with 2 wt% (Fig. 2 (II)). It was also observed that Pt deposition has a strong influence over the titania surface hydroxylation degree; thus, hydroxylation is lower on 0.5 wt%Pt–$TiO_2$ photocatalysts than on the photocatalysts prepared with the highest Pt content. This may be understood considering the large number of metallic particles homogeneously distributed over the $TiO_2$ surface in the former (Fig. 1(A)), which could reduce

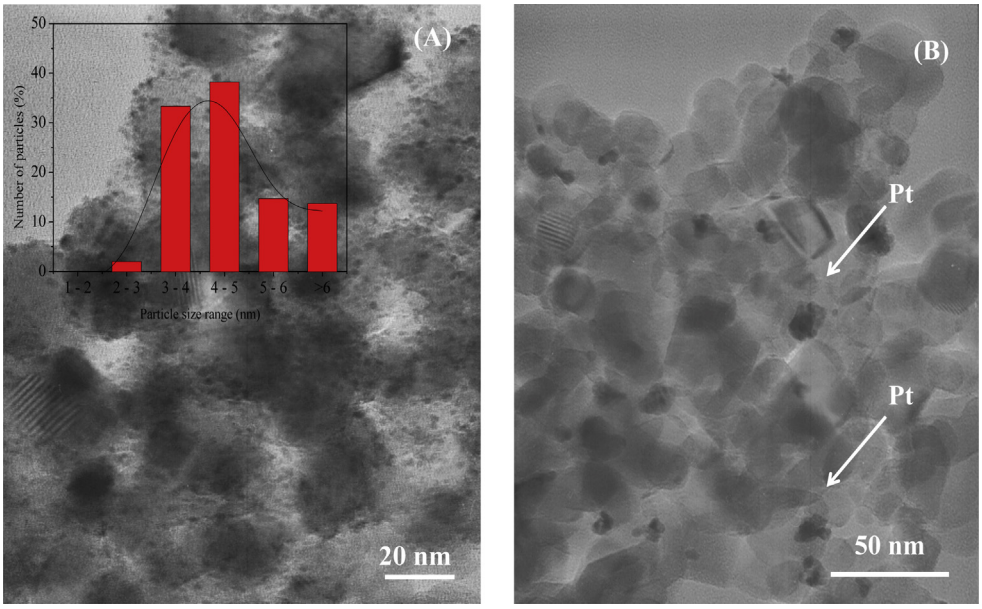


**Fig. 1.** TEM images and distribution of metal particle size of Pt–$TiO_2$ photocatalysts prepared with 120 min of deposition time and different platinum loading. (A) 0.5 wt% and (B) 2 wt%.

**Table 1**
Characterization results of $TiO_2$ and Pt–$TiO_2$ photocatalysts.

| | Deposition time (min) | $S_{BET}$ ($m^2$/g) | Pt (wt%) (XRF) | O/Ti | %$Pt^0$ | %$Pt^{\delta+}$ | $\bar{d}$ (nm) |
|---|---|---|---|---|---|---|---|
| $TiO_2$ | – | 58 | – | 1.70 | – | | – |
| 0.5 wt%Pt–$TiO_2$ | 15 | 48 | 0.23 | 1.89 | n.d. | n.d. | 2.9 |
| | 120 | 49 | 0.30 | 1.91 | n.d. | n.d. | 4.5 |
| | 240 | 45 | 0.33 | 1.86 | n.d. | n.d. | 5.9 |
| 2 wt%Pt–$TiO_2$ | 15 | 50 | 0.61 | 1.90 | 13 | 87 | n.d. |
| | 120 | 53 | 1.25 | 1.92 | 63 | 37 | n.d. |
| | 240 | 48 | 1.00 | 1.98 | 61 | 39 | n.d. |

n.d. not determined.

the number of available adsorption sites on the $TiO_2$ surface for OH groups or adsorbed water.

In the region between 1050 and 1250 $cm^{-1}$, IR bands assigned to sulfate species were detected in all the samples (Fig. 3(I) and (II)). The relative intensity of the sulfate groups bands in the 0.5 wt%Pt–$TiO_2$ photocatalysts (Fig. 3(I)) is higher than in the photocatalysts prepared with higher platinum content (Fig. 3(II)). As it can be seen in these figures, three clear bands located at 1045, 1124 and 1214 $cm^{-1}$ were detected in the $TiO_2$ spectrum. This may be attributed to the formation of a sulfate bidentate binuclear (bridging) surface complex on $TiO_2$ [25–27]. In the case of the platinized samples, four bands at higher wavenumbers are detected. The appearance of these bands could be interpreted as evidence of a bidentate coordination; however, the fourth band could also reflect the formation of a bisulfate or other protonated structures [26].

Brönsted and Lewis acid centers were also analyzed by FT-IR spectroscopy. Each sample was impregnated with vapor $NH_3$ dosed at room temperature for 30 min after what the infrared spectra were collected. FT-IR spectra obtained for pure $TiO_2$ and selected Pt–$TiO_2$ samples are presented in Fig. 4 (IR region between 1550 and 1150 $cm^{-1}$).

As it can be observed in the $TiO_2$ spectrum three low intensity IR bands located at 1450, 1331 and 1222 $cm^{-1}$ are clearly noticeable;

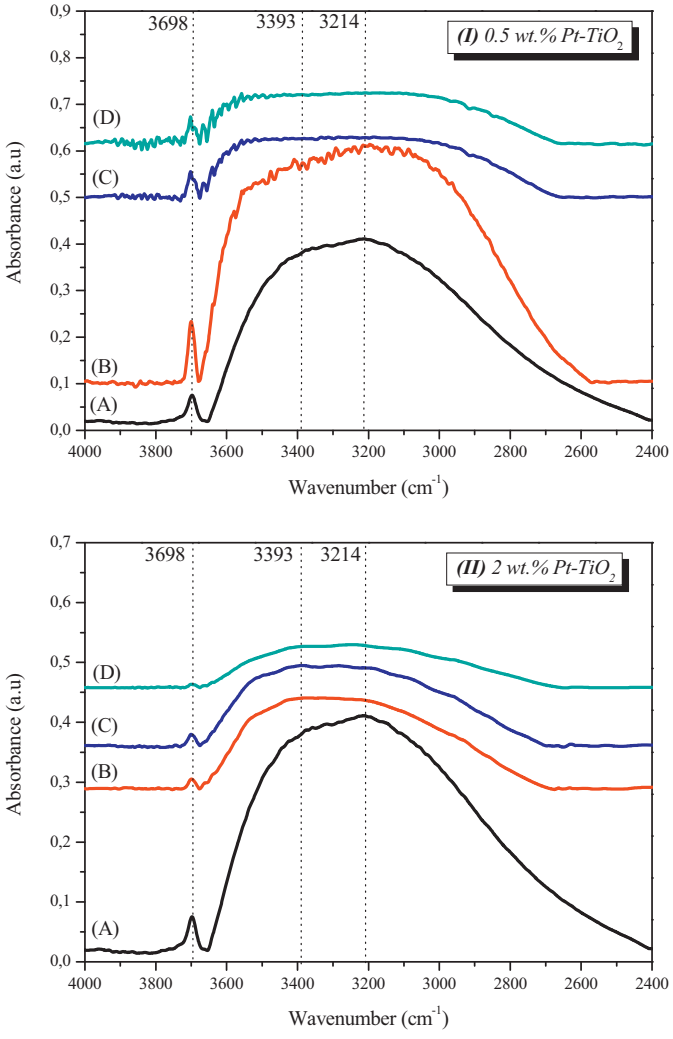


**Fig. 2.** IR spectra of the photocatalysts analyzed. (I) 0.5 wt% and (II) 2 wt%Pt loading. $TiO_2$ (A); and Pt–$TiO_2$ prepared with different deposition times: 15 min (B); 120 min (C) and 240 min (D). Hydroxyl groups region between 4000 and 2400 $cm^{-1}$.

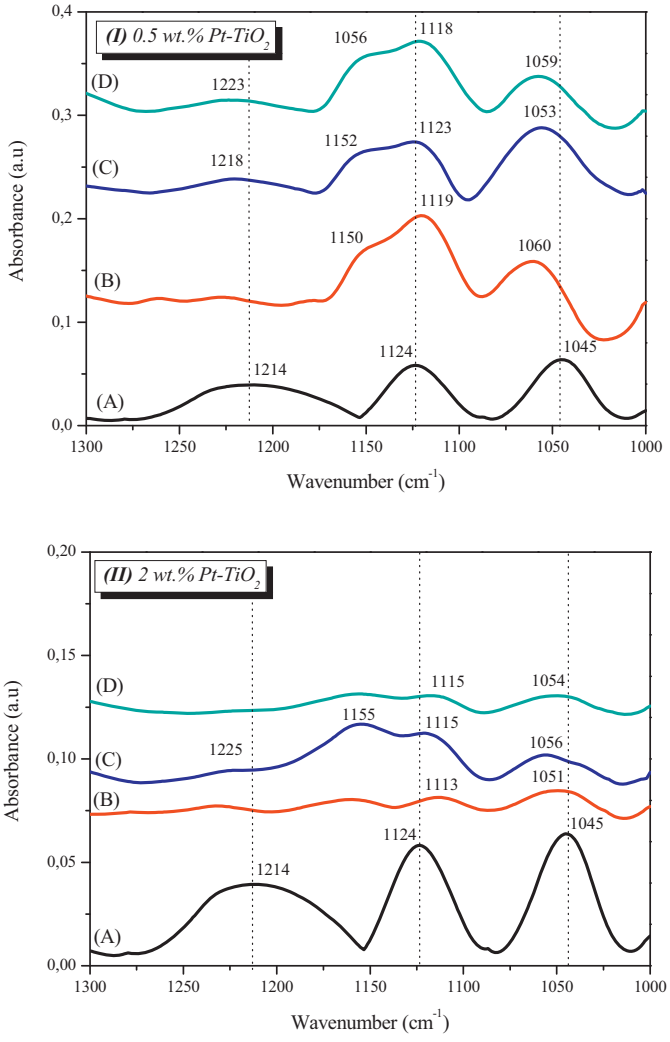


**Fig. 3.** IR spectra of the photocatalysts analyzed. (I) 0.5 wt% and (II) 2 wt%Pt loading. $TiO_2$ (A); and Pt–$TiO_2$ prepared with different deposition times: 15 min (B); 120 min (C) and 240 min (D). Surface sulfate groups region between 1300 and 1000 $cm^{-1}$.

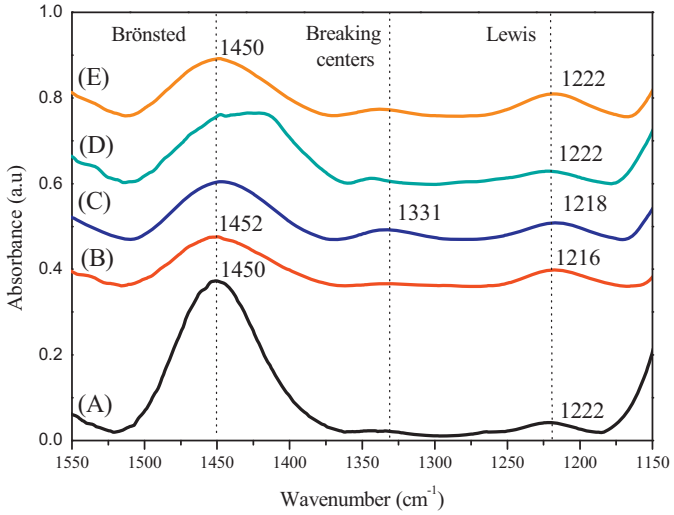


**Fig. 4.** Brönsted and Lewis sites in photocatalysts analyzed. $TiO_2$ (A); and Pt–$TiO_2$ prepared with different deposition times and metal loading: 0.5 wt% −15 min (B); 0.5 wt% −120 min (C); 2 wt% −15 min (D) and 2 wt% −120 min (E).

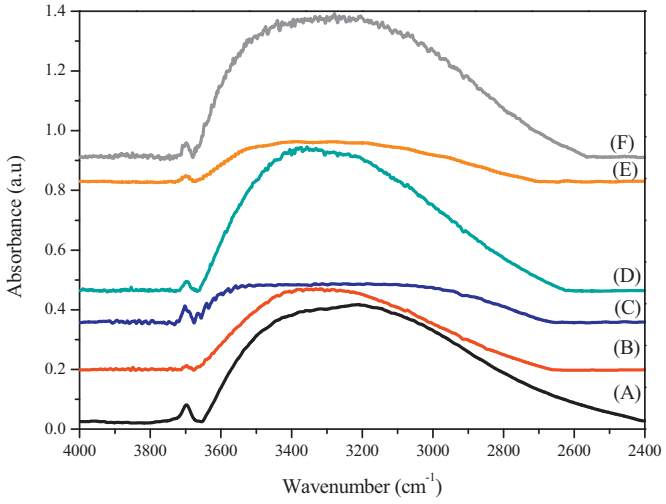


**Fig. 5.** IR spectra of the different photocatalysts unmodified and impregnated by phenol. $TiO_2$ (A); $TiO_2$ + Fenol (B); and Pt–$TiO_2$ prepared with 120 min of deposition time and different Pt loading: 0.5 wt%Pt (C); 0.5 wt%Pt + Fenol (D); 2 wt%Pt (E) and 2 wt%Pt + Fenol (F). IR region between 4000 and 2400 $cm^{-1}$.

these bands may be assigned to Brönsted sites, breaking centers and Lewis sites, respectively. A breaking center formation occurs in a surface on which coexist Brönsted and Lewis centers very close together, wherein the water molecule can be broken. A detailed explanation about breaking centers formation has been given in [29]. The relative intensity of the Brönsted center IR band in pure $TiO_2$ spectrum (Fig. 4, line (A)) is significantly higher than that of the Pt–$TiO_2$ photocatalysts, indicating a higher Brönsted acidity in pure $TiO_2$. This may be responsible for the differences observed in IR region between 3500 and 2400 $cm^{-1}$ (Fig. 2) where the hydroxyl groups can be seen.

On the other hand, platinum deposition leads to a slight growth of the breaking centers band (1331 $cm^{-1}$), being more intense in samples prepared with the highest deposition time; this fact is more noticeable in 0.5 wt%Pt–$TiO_2$ photocatalysts. These modifications in the relative intensity of the breaking centers band are probably due to the presence of strong Lewis acid centers close to Brönsted acid sites where the breaking of water molecules can take place [28,29].

### 3.3. Dark adsorption experiments

In Pt–$TiO_2$ materials there can be three different types of adsorption sites: Pt clusters, $Ti^{4+}$ and surface $OH^-$ groups [12]. The affinity of a given substrate with one or other of the adsorption sites may have a direct influence on the activity of the photocatalysts. In order to find a correlation between the adsorption of phenol and MO on the different samples and the photocatalytic behavior observed, a set of dark adsorption experiments was carried out. All the samples were impregnated with saturated solutions of phenol or MO and after impregnation and drying FT-IR measurements were performed.

#### 3.3.1. Phenol adsorption

Fig. 5 shows a comparison between the IR spectra of selected samples before and after impregnation with phenol (IR region between 4000 and 2400 $cm^{-1}$). As it can be seen, phenol impregnation produces some modifications in the relative intensity and in the amplitude of the IR bands. In the $TiO_2$ spectrum (Fig. 5, line (A)) it is possible to note that the relative intensity of the bands assigned to isolated hydroxyl groups (3698 $cm^{-1}$) and to H-bonded hydroxyl groups (region between 3500 and 2400 $cm^{-1}$) slightly decreases after phenol impregnation. In Pt–$TiO_2$ photocatalysts a quite different trend was observed. After phenol impregnation the relative intensity of the band assigned to H-bonded hydroxyl groups increases, this could be due to water adsorption on photocatalysts surfaces during phenol adsorption experiments; indicating an important difference in the lability of these bands between pure and metallized $TiO_2$. The modifications observed in the relative intensity and in the amplitude of the OH groups bands, demonstrates the presence of different adsorption centers in Pt–$TiO_2$ photocatalysts respect to $TiO_2$, probably surface Pt atoms.

Fig. 6 shows the IR spectrum of pure phenol in the range between 1700 and 1200 $cm^{-1}$. In this spectrum, three bands located at 1600, 1499 and 1473 $cm^{-1}$ are observed, assigned to $\nu$(CC) + [$\delta$(CH)] vibrations. The band at 1368 $cm^{-1}$ corresponds to $\delta$OH and the band located at 1233 $cm^{-1}$ is due to vibrational modes of $\nu$CO in the aromatic ring [30].

Fig. 7(I) and (II) shows the adsorption of phenol on $TiO_2$ and on Pt–$TiO_2$ photocatalysts prepared with different Pt content and deposition times (region between 1700 and 1200 $cm^{-1}$). As it can be seen, after phenol adsorption the band assigned to $\delta$OH vibration in phenol molecule has completely disappeared in the spectra of all samples, which may suggest the formation of phenolates

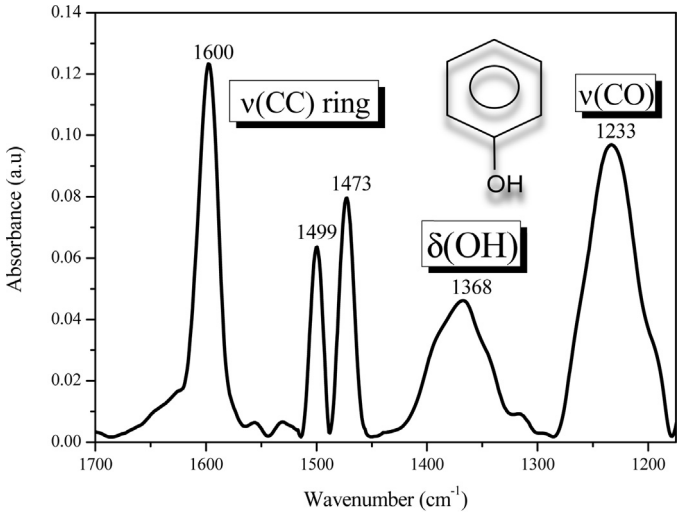


**Fig. 6.** Infrared spectrum of phenol.

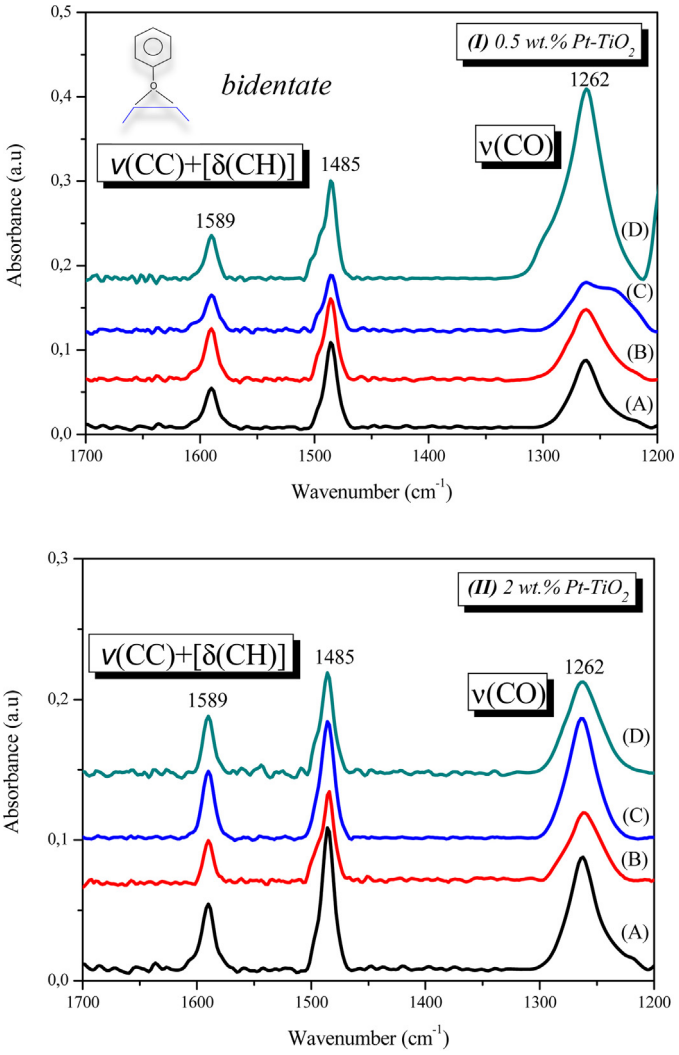


**Fig. 7.** IR spectra of the different photocatalysts impregnated by phenol. (I) 0.5 wt% and (II) 2 wt% Pt loading. $TiO_2$ (A); and Pt–$TiO_2$ prepared with different deposition times 15 min (B); 120 min (C) and 240 min (D).

on photocatalysts surfaces [28]. Only two bands located at 1589 and 1485 $cm^{-1}$ corresponding to $\nu$(CC) + [$\delta$(CH)] vibrations were observed. These bands are shifted to minor wavenumbers respect to phenol reference spectrum (Fig. 6). The band of $\nu$CO vibration is shifted 29 $cm^{-1}$ towards higher wavenumber values in all samples, compared to phenol reference spectrum (i.e. 1262 to 1233 $cm^{-1}$). It is also remarkable that for the 0.5 wt%Pt series, this band is wider compared to pure $TiO_2$; being more evident on the photocatalyst prepared with 240 min deposition time. In this catalyst the highest relative intensity of $\nu$CO vibration band was observed. All these modifications may indicate that on metalized samples phenol interaction takes place by the formation of bidentate phenolates species adsorbed on photocatalysts surfaces [30].

The role of platinum in phenol-photocatalysts interaction seems to be more intense in 0.5 wt%Pt–$TiO_2$ samples by increasing the deposition time (Fig. 7(I)). By contrast in 2 wt%Pt–$TiO_2$ series the IR spectra are very similar, without any apparent modifications due to deposition time (Fig. 7(II)). Taking into account that deposition time also affects the $Pt^0/Pt^{\delta+}$ fraction in platinized samples (Table 1), it is possible to think that both platinum content as its oxidation state can significantly influence the interaction of the phenol with the surface of these catalysts. Thus, bidentate phenolates may interact with surface $Ti^{4+}$ and $Pt^{\delta+}$ simultaneously.

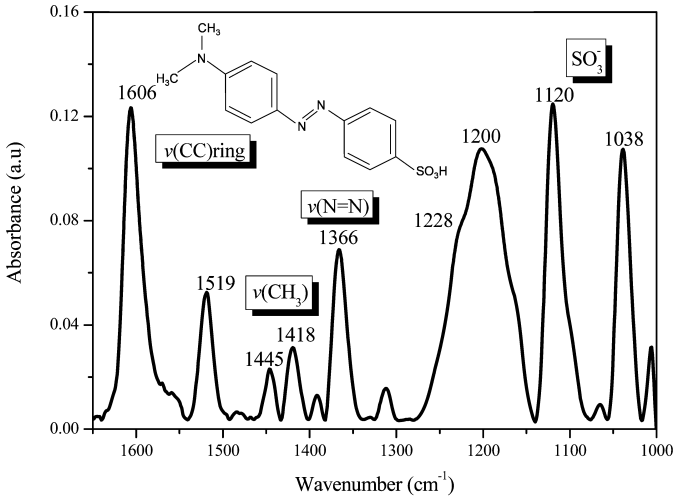


**Fig. 8.** Infrared spectrum of methyl orange.

### 3.3.2. Methyl orange adsorption

Fig. 8 shows the infrared spectrum of MO, the positions of characteristics IR bands of this dye have been indicated in the figure. Two bands located at ~1606 and 1519 $cm^{-1}$ are assigned to $\nu$CC vibrations in the aromatic rings; the bands at 1444 and 1415 $cm^{-1}$ corresponds to $\nu CH_3$ vibrations and a band located at 1366 $cm^{-1}$ is assigned to the azo group $\nu$N=N vibration. Bands assigned to sulfate groups from sulfonate species were also detected in the range between 1250 and 1000 $cm^{-1}$ [31].

In Fig. 9(I) and (II) the spectra of $TiO_2$ and Pt–$TiO_2$ photocatalysts after MO adsorption are presented. As it can be seen, MO adsorption leads to a decrease in the relative intensity of the band ascribed to $\nu$N=N vibration (1366 $cm^{-1}$) compared with the spectrum of pure MO (Fig. 8). This suggests that the adsorption of MO over $TiO_2$ surface is given by an interaction between the azo group (R–N=N–R) and $Ti^{4+}$ species. In general, the relative intensity of all MO adsorption bands is very similar between the spectra of Pt–$TiO_2$ samples prepared with low and high platinum loading (Fig. 9(I) and (II), respectively), thus indicating that Pt content does not influence importantly the MO adsorption. So, it is possible to think that MO interacts with only one adsorption center on photocatalysts surface, probably $Ti^{4+}$. These outcomes are different from those observed in the phenol adsorption; in the case of phenol, clear modifications in the relative intensity and in the amplitude of the IR bands with Pt loading were observed (Fig. 7). These differences have indicated that phenol interacts with $Ti^{4+}$ and $Pt^{\delta+}$ centers simultaneously (bidentate phenolate) as it was explained previously in Section 3.3.1.

It is important to note that the interaction of MO with Pt–$TiO_2$ photocatalyst surfaces through the azo group could be more favored than the interaction through amino group, due to the higher electron density provided by the double bond (N=N) in the former. Thus, the azo group acts as a strong base, which may interact easily with Brönsted and Lewis acid centers on $TiO_2$ and Pt–$TiO_2$ surface.

The interaction of the dye molecule with photocatalyst surface through its sulfonate ($SO_3^-$) group cannot be ruled out; since modifications in the wavenumber of the bands located in the region between 1250 and 1000 $cm^{-1}$ were also observed; however, the presence of sulfates groups adsorbed on surface and coming from sulfate pre-treatment of the materials did not allow us to determine accurately the position and/or the modifications of the sulfonate band in the photocatalysts.

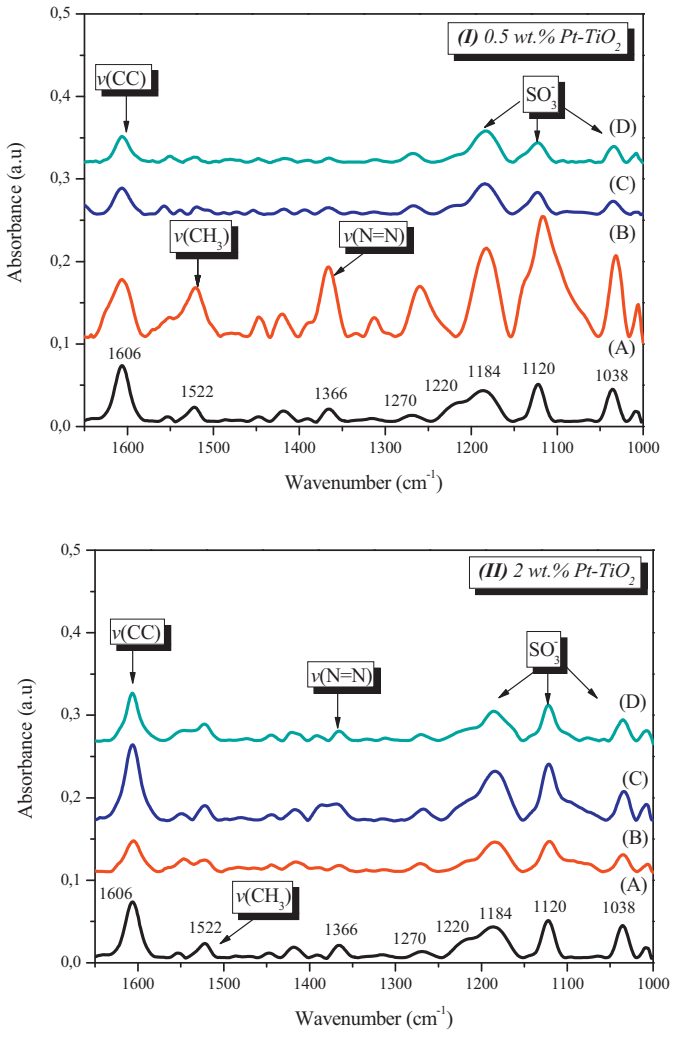


**Fig. 9.** IR spectra of the different photocatalysts impregnated by MO. (I) 0.5 wt% and (II) 2 wt%Pt loading. $TiO_2$ (A); and Pt–$TiO_2$ prepared with different deposition times: 15 min (B); 120 min (C) and 240 min (D) of deposition time. IR region between 1650 and 1000 $cm^{-1}$.

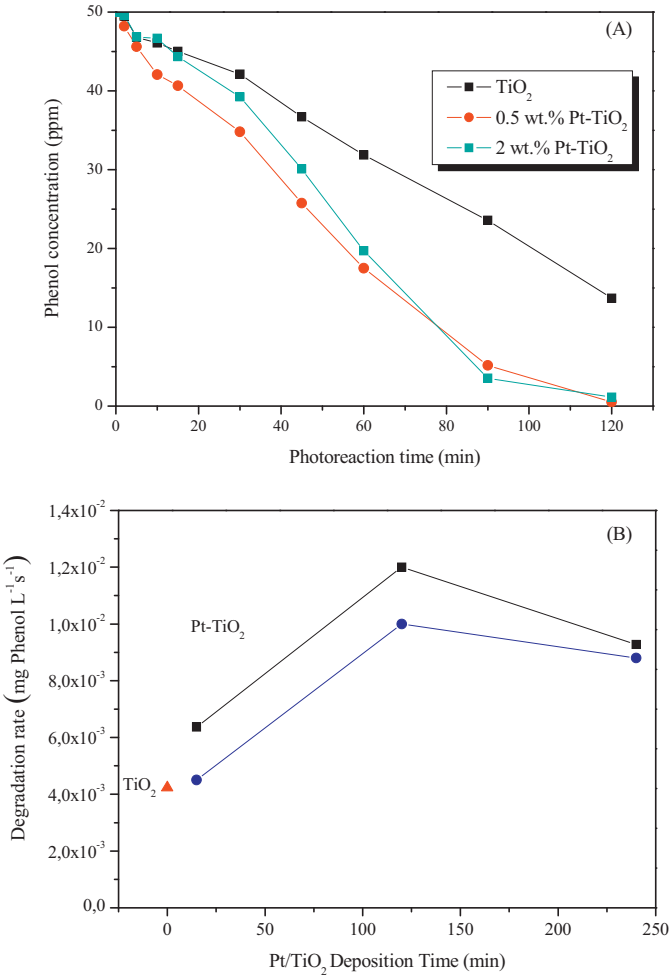


**Fig. 10.** (A) Evolution of the substrate concentration during phenol photodegradation over $TiO_2$ and Pt–$TiO_2$ photocatalysts prepared at 120 min of deposition time. (B) Initial reaction rates for phenol photo-oxidation (mg of phenol per liter and second) over the different photocatalysts, as a function of deposition time. (▲) $TiO_2$; (■) 0.5 wt%Pt–$TiO_2$ and (●) 2 wt%Pt–$TiO_2$.

### 3.4. Photocatalytic activity of $TiO_2$ and Pt–$TiO_2$ photocatalysts

#### 3.4.1. Phenol photo-degradation

Fig. 10(A) shows the evolution of phenol concentration during the photooxidation of this substrate over the $TiO_2$ and the Pt–$TiO_2$ photocatalysts. As it can be observed, phenol concentration decreases progressively with photoreaction time; thus, the total elimination of phenol was achieved over the 0.5 wt%Pt–$TiO_2$ photocatalyst after 2 h of reaction time.

Initial reaction rates for phenol photo-oxidation over $TiO_2$ and Pt–$TiO_2$ photocatalysts are plotted in Fig. 10(B). As can be seen, the lowest photo-activity was obtained on pure $TiO_2$ (i.e. $4.23 \times 10^{-3}$ mg phenol/L s). In general, the addition of platinum significantly increased the photocatalytic activity of $TiO_2$ in phenol oxidation. The more remarkable improvement in $TiO_2$ photo-activity was achieved by addition of 0.5 wt%Pt nominal content; and a further increase of metal content to 2 wt% had a detrimental effect on catalyst photo-activity. Moreover, it was observed that photodeposition time had also a considerable influence on the phenol photo-degradation rate; thus, the highest photocatalytic activity was obtained over the 0.5 wt%Pt–$TiO_2$ photocatalyst prepared with 120 min of deposition time (i.e. an initial reaction rate of $1.2 \times 10^{-2}$ mg phenol/L s). A fall in photo-activity was observed over photocatalysts prepared with longer deposition times.

It is generally accepted that $TiO_2$ protoefficiency can be improved by platinum deposition. This has been mainly ascribed to a better separation of the electron–hole pairs photogenerated; the Pt deposits act as a trap for electrons, thus decreasing the recombination rate. However, as it was described in section 3.3.1, Pt deposits might also play an important role in the mechanism and in the intensity of the substrate-photocatalyst surface interaction. In this work it has been observed that the photodeposition of 0.5 wt% nominal Pt content on $TiO_2$ not only reduces the electron–hole pairs recombination, but also leads to increase the adsorption of phenol on photocatalyst surface. Moreover, as it was indicated in Section 3.3.1, it seems to be that adsorbed water is more labile in Pt–$TiO_2$ photocatalysts than on pure $TiO_2$. These conditions may favor the access of the phenol molecule to the photocatalyst surface during the photocatalytic reaction; which results in a more effective photo-degradation process.

#### 3.4.2. Methyl orange photo-degradation

Fig. 11(A) shows the evolution of MO concentration during the photo-oxidation of this substrate over $TiO_2$ and Pt–$TiO_2$ photocatalysts. As it can be seen, dye concentration decreases progressively

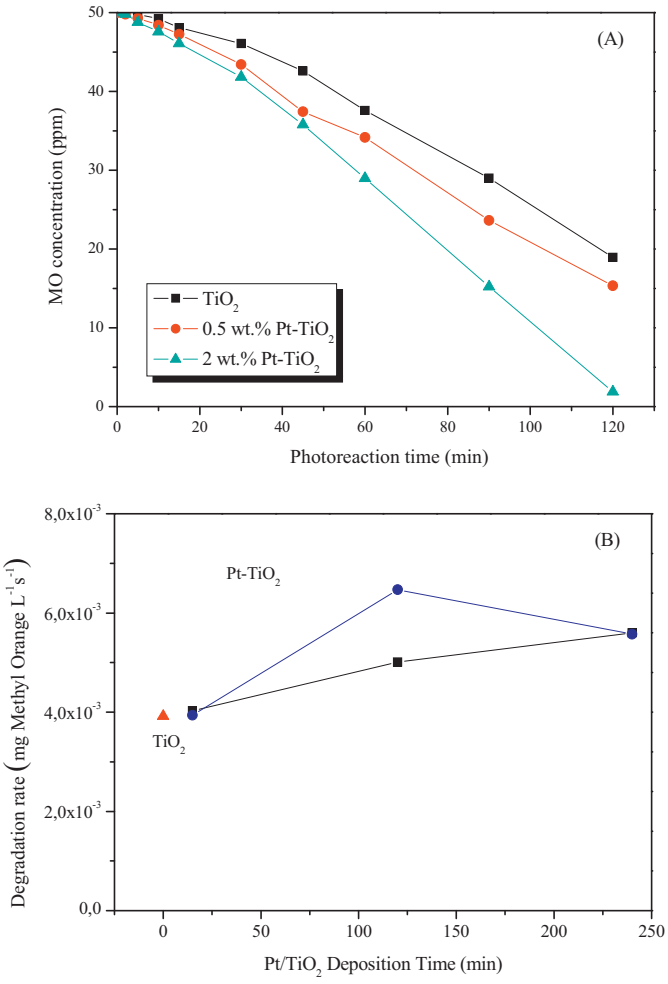


**Fig. 11.** (A) Evolution of substrate concentration during MO photodegradation over $TiO_2$ and Pt–$TiO_2$ photocatalysts prepared at 120 min of deposition time. (B) Initial reaction rates for methyl orange photo-degradation (mg of MO per liter and second) over the different photocatalysts, as a function of deposition time. (▲) $TiO_2$; (■) 0.5 wt%Pt–$TiO_2$ and (●) 2 wt%Pt–$TiO_2$.

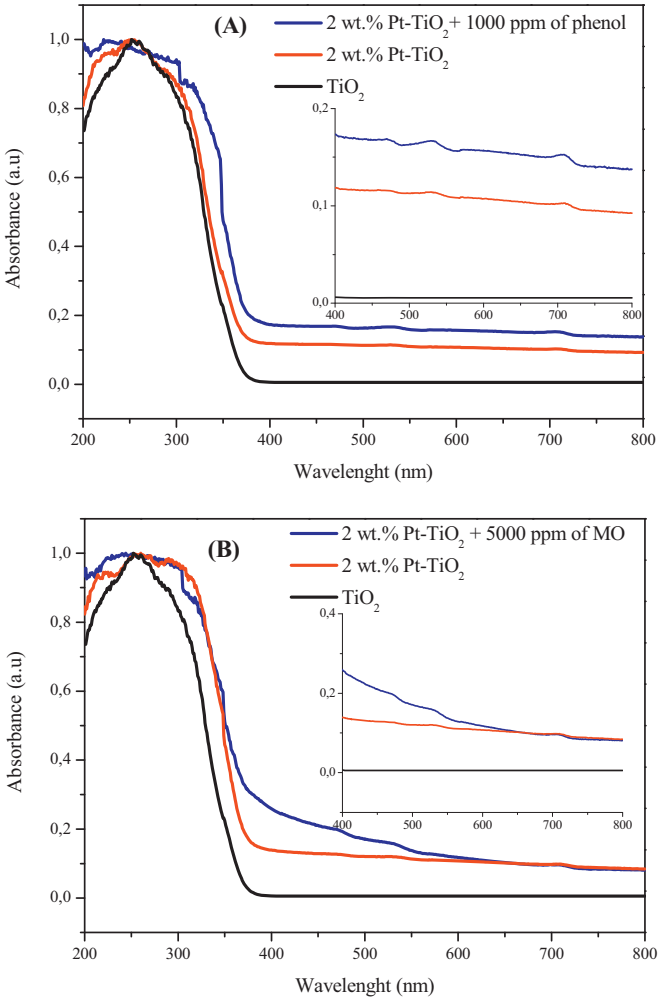


**Fig. 12.** UV–vis DRS spectra collected before and after phenol (A) or methyl orange (B) impregnation on 2 wt%Pt–$TiO_2$ photocatalyst prepared with 120 min of deposition time.

with photoreaction time. No deactivation of the photocatalysts was observed even after 100 min of reaction time.

The relation between platinum content and MO photo-degradation rate is presented in Fig. 11(B). An important increase of $TiO_2$ photoactivity by Pt deposition was observed. As it can be seen in this figure, the MO degradation rate is higher on 2 wt%Pt–$TiO_2$ than on 0.5 wt%Pt–$TiO_2$ photocatalysts.

It has been widely reported that Pt particle size strongly affects the photocatalytic activity of platinized $TiO_2$. Thus, it is generally accepted that the addition of small Pt particles leas to better photoactivity results than the addition of large Pt particles, which can have even a detrimental effect over $TiO_2$ efficiency [19,32,33]. However, in this work a very different behavior was observed, since the highest MO photo-degradation rate was obtained over 2 wt%Pt–$TiO_2$ photocatalysts; where the largest platinum particle size among all the series of photocatalysts analyzed was found. This behavior can be explained taking into account that, as it has been indicated in section 3.3.2, MO adsorption on $TiO_2$ takes place mainly through the interaction between the azo group of the dye molecule and the $Ti^{4+}$ species on titania surface. The 0.5 wt%Pt–$TiO_2$ photocatalysts presented the smallest Pt particle size which can importantly reduce electron–hole recombination; however, at the same time, in these materials the Pt particles are homogeneously covering the $TiO_2$ surface; hindering the azo–$Ti^{4+}$ interaction.

On the other hand, the photocatalysts prepared with 2 wt% of nominal platinum content presented larger metal particle sizes than the series with 0.5 wt% of Pt. So, in 2 wt%Pt–$TiO_2$ series, the aggregation of platinum deposits may favor the access of the dye molecule to $TiO_2$ surface, making easier the azo–$Ti^{4+}$ interaction. This can explain the best photo-degradation rate of MO observed over the 2 wt%Pt–$TiO_2$ photocatalysts. Moreover, the highest water lability on Pt–$TiO_2$ surface may also play an important role MO photo-degradation, as it has also been observed in the case of phenol.

In the present work UV–vis DRS spectra of Pt–$TiO_2$ photocatalysts were collected before and after phenol or MO impregnation; these spectra are included in Fig. 12(A) and (B), respectively. As it can be observed, the absorption of the Pt–$TiO_2$ samples in the visible region is higher than in pure $TiO_2$, due to a decrease in reflectivity evidenced by the dark gray color of platinized samples. After impregnation with phenol or MO, the absorption of Pt–$TiO_2$ samples in the visible region increases further. From these results it is possible to think that $Pt^{\delta+}$ species are also involved in substrate-photocatalysts interactions probably giving rise to the formation of substrate-$Pt^{\delta+}$ surface complexes. The charge transfer from MO to oxidized platinum species may be responsible of the further increase of the absorption in the range between 400 and 800 nm.

## 4. Conclusions

Platinum content and deposition time are the main factors influencing the Pt particle size and dispersion in Pt–$TiO_2$ photocatalysts prepared by photodeposition method. Photocatalytic activity of $TiO_2$ for phenol and MO degradation was improved by Pt addition in any case; this enhancement has been ascribed not only to a lower recombination rate but also to an important improvement of substrate–$TiO_2$ surface interaction.

Adsorption of phenol on $TiO_2$ and Pt–$TiO_2$ photocatalysts takes place mainly through the formation of bidentate phenolates species. These species interact preferentially with Pt deposits on $TiO_2$ surface. Thus, a large number of small Pt deposits homogeneously distributed on $TiO_2$ surface could favor phenol–photocatalyst interaction, thus improving the phenol degradation rate. Due to this, 0.5 wt%Pt–$TiO_2$ photocatalysts presented the best photoactivity phenol photo-degradation. The oxidation state of Pt and simultaneous interaction between phenol and $Ti^{4+}$ and $Pt^{\delta+}$ centers seems to be determinant in the bidentate phenolate formation.

The MO adsorption on Pt–$TiO_2$ photocatalysts surface takes place preferentially through the interaction of the azo group (N=N) with $Ti^{4+}$ on $TiO_2$ surface. In 2 wt%Pt–$TiO_2$ photocatalysts, Pt deposits present a higher aggregation degree, thus there is a higher extension of $TiO_2$ surface not covered by Pt deposits, which may favor the azo–$Ti^{4+}$ interaction improving the efficiency of the photocatalytic process. The best photocatalytic performance of these materials in MO photo-degradation is due to a combined effect between the suitable separation of photogenerated charges induced by Pt and a improvement of MO adsorption. Here we can find the reason for the better photocatalytic behavior of the series with larger Pt particle sizes.

## Acknowledgments

This research was financed by the Spanish Ministerio de Ciencia e Innovación (Project Ref. CTQ2011-26617-C03-02). J.J. Murcia would like to thank CSIC for the concession of a JAE grant and for financing the short stay No. 2012ESTCSIC - 7731. CITIUS (University of Seville) is acknowledged for XPS and XRF measurements.

## References

[1] A.V. Vorontsov, E.N. Savinova, J. Zhensheng, J. Photochem. Photobiol., A 125 (1999) 113–117.
[2] M. Qamar, Int. J. Nanosci. 9 (2010) 579–583.
[3] J. Lee, W. Choi, J. Phys. Chem. B 109 (2005) 7399–7406.
[4] J.J. Murcia, J.A. Navío, M.C. Hidalgo, Appl. Catal., B 126 (2012) 76–85.
[5] J.J. Murcia, M.C. Hidalgo, J.A. Navío, V. Vaiano, P. Ciambelli, D. Sannino, Int. J. Photoenergy 2012 (2012), Article ID 687262, 9 pages.
[6] J.J. Murcia, M.C. Hidalgo, J.A. Navío, V. Vaiano, P. Ciambelli, D. Sannino, Catal. Today 196 (2012) 101–109.
[7] E. Sanchez, T. Lopez, Mater. Lett. 25 (1995) 271–275.
[8] D. Sannino, V. Vaiano, P. Ciambelli, M.C. Hidalgo, J.J. Murcia, J.A. Navio, J. Adv. Oxid. Technol. 15 (2013) 284–293.
[9] D. Sannino, V. Vaiano, P. Ciambelli, J.J. Murcia, M.C. Hidalgo, J.A. Navio, J. Adv. Oxid. Technol. 16 (2013) 71–82.
[10] F.B. Li, X.Z. Li, Chemosphere 48 (2002) 1103–1111.
[11] W. Choi, A. Termin, M.R. Hoffmann, J. Phys. Chem. 98 (1994) 13669–13679.
[12] A.V. Vorontsov, I.V. Stoyanova, D.V. Kozlov, V.I. Simagina, E.N. Savinov, J. Catal. 189 (2000) 360–369.
[13] W.Y. Teoh, L. Mädler, R. Amal, J. Catal. 251 (2007) 271–280.
[14] F. Denny, J. Scott, K. Chiang, W.Y. Teoh, R. Amal, J. Mol. Catal. A: Chem. 263 (2007) 93–102.
[15] C. Hu, Y. Tang, Z. Jiang, Z. Hao, H. Tang, P.K. Wong, Appl. Catal., A 253 (2003) 389–396.
[16] S.P. Tandom, J.P. Gupta, Phys. Status Solidi B 38 (1970) 363–367.
[17] University of Leipzig, Germany, www.uni-leipzig.de/~unifit
[18] L.C. Chen, F.R. Tsai, C.M. Huang, J. Photochem. Photobiol., A 170 (2005) 7–14.
[19] M.C. Hidalgo, M. Maicu, J.A. Navío, G. Colón, Appl. Catal., B 81 (2008) 49–55.
[20] I. Carrizosa, G. Munuera, J. Catal. 49 (1977) 174–188.
[21] A.J. Maira, J.M. Coronado, V. Augugliaro, K.L. Yeung, J.C. Conesa, J. Soria, J. Catal. 202 (2001) 413–420.
[22] J. Araña, J.M. Doña-Rodríguez, O. González-Díaz, E. Tello Rendón, J.A. Herrera Melián, G. Colón, J.A. Navío, J. Pérez Peña, J. Mol. Catal. A: Chem. 215 (2004) 153–160.
[23] P.A. Connor, K.D. Dobson, A.J. McQuillan, Langmuir 15 (1999) 2402–2408.
[24] M. Takeuchi, G. Martra, S. Coluccia, M. Anpo, J. Phys. Chem. C 111 (2007) 9811–9817.
[25] D. Peak, R.G. Ford, D.L. Sparks, J. Colloid Interface Sci. 218 (1999) 289–299.
[26] S.J. Hug, J. Colloid Interface Sci. 188 (1997) 415–422.
[27] T. Yamaguchi, Appl. Catal. 61 (1990) 1–25.
[28] L. Qingya, L. Zhenyu, L. Chengyue, Chinese J. Catal. 27 (2006) 636–646.
[29] J.J. Murcia, M.C. Hidalgo, J.A. Navío, J. Araña, J.M. Doña-Rodríguez, Appl. Catal., B 142 (2013) 205–213.
[30] A. Popov, E. Kondratieva, J.P. Gilson, L. Mariey, A. Travert, F. Maugé, Catal. Today 172 (2011) 132–135.
[31] R. Gup, E. Giziroglu, B. Kirkan, Dyes Pigm. 73 (2007) 40–46.
[32] S. Gan, Y. Liang, D.R. Baer, M.R. Sievers, G.S. Herman, C.H.F. Peden, J. Phys. Chem. B 105 (2001) 2412–2416.
[33] M.C. Hidalgo, M. Maicu, J.A. Navío, G. Colón, Catal. Today 129 (2007) 43–49.